Energy Evolution, Stabilization, and Mechanotransducer Properties of Fe_3O_4 Vortex Nanorings and Nanodisks

Gopal Niraula,[1,2] Denilson Toneto,[3] Elma Joshy,[4] Jose A. H. Coaquira,[2] Ahmad I. Ayesh,[5,6] Flavio Garcia,[7] Diego Muraca,[8] Juliano C. Denardin,[9] Gerardo F. Goya,[10] and Surender K. Sharma[1,4,*]

[1] *Department of Physics, Federal University of Maranhao, Sao Luis 65080-805, Brazil*
[2] *Laboratory of Magnetic Materials, NFA, Institute of Physics, University of Brasilia, Brasilia 70910-900, Brazil*
[3] *Departamento de Física, Universidade Federal de Santa Maria, UFSM, Santa Maria, RS 97105-900, Brazil*
[4] *Department of Physics, Central University of Punjab, Bathinda, 151401, India*
[5] *Center for Sustainable Development, Qatar University, P.O. Box 2713, Doha, Qatar*
[6] *Department of Mathematics, Statistics and Physics, Qatar University, P.O. Box 2713, Doha, Qatar*
[7] *Brazilian Center for Research in Physics - CBPF, Rio de Janeiro - RJ, 22290-180, Brazil*
[8] *Institute of Physics "Gleb Wataghin" (IFGW), University of Campinas, Campinas, Brazil*
[9] *CEDENNA and Departamento de Física, Universidad de Santiago de Chile (USACH), Santiago 9170124, Chile*
[10] *Instituto de Nanociencia y Materiales de Aragón (INMA), Universidad de Zaragoza, 50018, Zaragoza, Spain*

(Received 24 March 2021; revised 23 June 2021; accepted 12 July 2021; published 2 August 2021)

Recent reports on spin structures produced in nanomaterials due to confinement of spins imposed by geometrical restrictions are at the center of rising scientific interest. Topological curling magnetic structures (vortices) exhibit unique properties, regarding the energy profile, good colloidal stability in suspensions, manipulation under a low-frequency magnetic field, and torque exertion. The last property provides the potential to mechanically eradicate cancer cells via magnetomechanical actuation using remote ac magnetic fields. Here, we study, theoretically and by micromagnetic simulations, the magnetic energy evolutions for vortex nanosystems, i.e., Fe_3O_4 nanodisks (NDs) and nanorings (NRs). The obtained results for magnetic energy, magnetic susceptibility, and magnetization reversal confirm that the vortex-domain structure in NRs exhibits better stability and avoids agglomeration in solution, owing to the presence of a central hole, whereas the presence of a vortex core in NDs induces magnetic remanence. Although NDs are found to exert slightly higher torques than NRs, this weakness can be compensated for by a small increase (i.e., approximately equals 20%) in the amplitude of the applied field. Our results provide evidence of the magnetic stability of the curling ground states in NRs and open the possibility of applying these systems to magnetomechanical actuation on single cells for therapeutics in biomedicine, such as cancer-cell destruction by low-frequency torque transduction.

DOI: 10.1103/PhysRevApplied.16.024002

I. INTRODUCTION

The capability of a magnetic field to safely permeate human organs and interact with magnetic nanoparticles provides promising routes for therapies and diagnostics in biomedicine [1–6]. Among these routes, the transduction of the magnetic interaction of an external ac field and magnetic nanosystems into magnetomechanical actuation makes it possible to mechanically destroy previously targeted cells, bacteria, or other unicellular organisms. The physical mechanisms involved are based on the torque induced by nanoparticles under the rotation effect of a low-frequency (i.e., few-Hz frequency) ac magnetic field, which mechanically actuates cells [7–9]. This torque can be exploited in several ways to trigger receptors connected with cell death, open ion channels, or transfer direct physical spoilage to cells and has been shown to result in cell death both *in vitro* and *in vivo*. For instance, it has been reported that the oscillation of magnetic nanoparticles can induce calcium influx from membrane ionic channels or calcium casting from internal cell origins, which results in perturbation of cellular calcium homeostasis and stimulates the apoptosis process [10–12].

Magnetic nanoparticles with vortex structures provide a stable configuration that can rotate with the application of an external field. The magnetic field suffices for a magnetization process that generates a large magnetic moment in these systems due to the high intrinsic magnetization,

*surender76@gmail.com

allowing their manipulation even by a weak external magnetic field. One advantage of the vortex configuration over the simple single-domain magnetic structure is that it can show negligible dipole-dipole interactions, and thus, negligible magnetic remanence, allowing the magnetic nanosystems to remain well dispersed in colloidal formulations in the absence of an exterior magnetic field. Recently, the possible use of magnetic vortex microdisks (MDs) and nanodisks (NDs) for *in vitro* experiments with glioma cancer cells and mechanosensory cells has been studied under weak and slow magnetic fields, suggesting that vortex disks are excellent mechanotransducers compared with superparamagnetic nanoparticles for eradicating cancer cells [11,12]. An important result relates to the significant remanent magnetization (M_R) in these systems, due to the presence of a central vortex core that gives out-of-plane magnetization in NDs; such M_R significantly contributes to agglomeration of NDs in suspensions [13]. The M_R distribution is a complex phenomenon that relies on the size and shape of the particle, as well as on the balance of different energy contributions to the magnetic energy. The zero-field vortex configuration is specified by the balance between the exchange and magnetostatic energies, which can be controlled by the defined geometry, i.e., the thickness and diameter of the vortex nanosystem; in the vortex state, the total energy is almost dominated by the exchange energy because of the formation of a central vortex in NDs [14]. Upon decreasing the disk diameter at a constant thickness, the comparative contribution of the exchange energy of the central vortex surges and renders the vortex state less stable and lower than the critical diameter. It is worth noting that the M_R of NDs is higher near the critical size (closer to the single-domain region). Such M_R can be reduced to zero by increasing the diameter of NDs to within 0.5–1 μm, but this size limits the use of NDs in biomedicine [15,16]. On the other hand, the absence of a central vortex core substantially reduces the exchange energy in NRs, making their vortex state energetically favorable, i.e., the lowest-energy state (ground state), without out-of-plane magnetization ($M_R = 0$), which avoids possible agglomeration in suspensions [14,17]. In addition, vortex NRs have lower energy than NDs and do not produce surface magnetostatic charges, thus becoming more stable. It is clear that an understanding of the energy evolution in defined magnetic vortex nanosystems and its stabilization is a crucial factor to examine the possibility of using such systems in biomedicine. One great advantage of NRs over NDs is that the vortex state is always an energetically lower state in NRs, whereas it is an energetically lower state only above a critical size in NDs [14]. Thus, in this scenario, a strategy can be envisaged in which vortex NRs are used as magnetomechanical transducers for cancer-cell destruction.

Here, we report a numerical study on the vortex states in nanorings (NRs) and nanodisks (NDs) using a theoretical model and micromagnetic simulations of the exchange and magnetostatic energies and their contribution to the total magnetic energy of the system. We also analyze how such magnetic energy evolves from the ND topology to the NR topology. From our results on the energy and magnetic susceptibility of these configurations, the dispersion and agglomeration effects in the colloidal state are discussed. Finally, the magnetomechanical properties of NRs and NDs under a very low field (<250 Oe) are compared. Our results show that the vortex NR magnetic configuration might potentially be used to perform mechanical actuation at the nanoscale, particularly as a nanotransducer, to produce mechanical damage on targeted cells in biomedical therapeutics.

II. MICROMAGNETIC MODELING

A. Micromagnetic simulation

The micromagnetic simulation is performed by the Mumax 3.9 package. Within this package, the time evolution of the magnetization allocation is obtained by solving the Landau-Lifshitz-Gilbert-Langevin equation:

$$\frac{\partial \vec{M}(r,t)}{\partial t} = \frac{-\gamma}{1+\alpha^2}\vec{M}(r,t) \times \overrightarrow{H}_{\text{eff}} - \frac{\gamma\alpha}{(1+\alpha^{\,2})M_S}\vec{M}(r,t)[\vec{M}(r,t) \times \overrightarrow{H}_{\text{eff}}], \quad (1)$$

where

$$\overrightarrow{H}_{\text{eff}} = \frac{\partial E_{\text{tot}}}{\partial M_S}. \quad (2)$$

Here, $M(r, t)$ is the magnetization distribution, H_{eff} is the effective field, M_S is the saturation magnetization, and γ is the gyromagnetic percentage ($=1.78 \times 10^{11}$ $\text{s}^{-1}\,\text{T}^{-1}$). The full energy ($E_{\text{tot}}$) is the addition of five energy terms, the exchange, self-magnetostatic, magnetocrystalline anisotropy, surface anisotropy, and Zeeman, where the exchange and magnetostatic energies are crucial in vortex systems.

The magnetic parameters of Fe_3O_4 used in the micromagnetic simulation are the maximum saturation magnetization, $M_S = 480$ kA/m; the exchange stiffness constant, $A = 1.2 \times 10^{-11}$ J/m; and the magnetocrystalline anisotropy constants, $K_1 = -1.35 \times 10^4$ J/m^3 and $K_2 = -0.44 \times 10^4$ J/m^3. The lateral cell size is $5 \times 5 \times 5$ nm^3; this lateral size (5 nm) is less than the exchange length, L_{ex} ($\approx$10.7 nm), as expressed by $L_{\text{ex}} = (2A/\mu_O M_S^2)^{0.5}$, to ensure the high accuracy of the simulation, and the Gilbert damping coefficient is set to $\alpha = 0.5$ [18,19].

B. Construction of the phase diagram

We investigate the low-energy configurations as a function of thickness, t, and diameter, d, of NDs and as a

function of thickness, t, and internal diameter, d_{in}, at constant external diameter, d_{out}, of NRs. The system is relaxed to a local energy minimum, and the final spin arrangement and the lower-energy states in both types of system, i.e., NDs and NRs, are studied. Thereafter, we compare the relative energy of each final configuration and select as a ground state the state with a low energy value. This process is repeated for many diameters and thicknesses, and the phase diagram is structured as a function of the dimension. In the case of NDs, three idealized main characteristic configurations are found: (i) in-plane single domain (planar); (ii) out-of-plane single domain (perpendicular); and (iii) vortex state, in that most of the magnetic moments are parallel to the plane of NDs. In contrast, in NRs, four idealized characteristic configurations are found: (i) in-plane single domain, (ii) in-plane flower state, (iii) vortex state, and (iv) helix state.

III. THEORETICAL MODEL

A. Construction of the phase diagram for NDs

We use two different expressions proposed by Altbir Drullinsky *et al.* [20] to construct the complete phase diagram separating the in-plane single domain (SD), out-of-plane SD, and vortex as the ground state in NDs: (i) the transition between in-plane and vortex phases is obtained by applying the expression $R = 9.82(L_{\text{ex}}^2/t) + 2.37L_{\text{ex}}$, and (ii) the transition between out-of-plane and vortex phases is obtained by the expression $R = L_{\text{ex}}(t/0.082L_{\text{ex}})^{0.3}$, where R, L_{ex}, and t are the radius, exchange length, and thickness, respectively.

We theoretically describe the ground states in magnetic nanodots, providing explicit expressions to calculate the transition lines among vortex and SD states.

B. Construction of the phase diagram for NRs

Furthermore, we use the expression $R = 9.82[L_{\text{ex}}^2 t/\alpha(\beta)]^{0.33}$, as collectively proposed by Landeros *et al.* [21] and Escrig *et al.* [22], to construct a phase diagram for NRs, where L_{ex} and t are the exchange length and thickness, respectively, and $\alpha(\beta)$ is a transition function that separates the uniform state and vortex state.

C. Exchange energy

The magnetic vortex state can be energetically preferable only when the particle size is greater than the exchange length, L_{ex}. In the case of the vortex state, the magnetostatic energy is zero, and the only energy value is the exchange energy; this structure has cylindrical symmetry. The exchange energy, E_{ex}^V, in the vortex state is given by [19,23]

$$E_{\text{ex}}^V = \frac{\mu_O M_S^2 2L_{\text{ex}}^2}{2(R_{\text{out}}^2 - R_{\text{in}}^2)} \ln \frac{R_{\text{in}}}{R_{\text{out}}} \quad \text{for NRs,} \tag{3}$$

$$E_{\text{ex}}^V = \frac{\mu_O M_S^2 2L_{\text{ex}}^2}{2(R_{\text{out}}^2 - R_{\text{in}}^2)} \ln \frac{R_{\text{out}}}{R_{\text{in}} + 0.5L_{\text{ex}}} \quad \text{for NDs,} \tag{4}$$

where R_{out} and R_{in} are the outer and inner radii, respectively.

Since the extra exchange energy, E_{ex}^r, term appears because of the edge roughness, which is proportional to the ratio between the perimeter and the volume of the ring,

$$E_{\text{ex}}^r \frac{2\pi(R_{\text{out}} + R_{\text{in}})t\sigma}{\pi(R_{\text{out}}^2 - R_{\text{in}}^2)t} = \frac{2\sigma}{W},$$

which can be further written as

$$E_{\text{ex}}^r = \frac{\mu_O M_S^2 C_O^{\text{ex}} R_{\text{out}} t}{2L_{\text{ex}}^2} \frac{2\sigma}{W}, \tag{5}$$

where $C_O^{\text{ex}} = 9.2 \times 10^{-6}$ is a characteristic energy for such nanostructures, $w = R_{\text{out}} - R_{\text{in}}$ is the width, and σ is the roughness amplitude. For a disk, $w = R_{\text{out}} - R_{\text{in}} = R_{\text{out}}$, since $R_{\text{in}} = 0$. Therefore, the total exchange energies of ring and disk elements with the edge-roughness-energy contribution become

$$E_{\text{ex}}^{\text{tot}} = E_{\text{ex}}^V + E_{\text{ex}}^r = \frac{\mu_O M_S^2 2L_{\text{ex}}^2}{2(R_{\text{out}}^2 - R_{\text{in}}^2)} \ln \frac{R_{\text{out}}}{R_{\text{in}}} + \frac{\mu_O M_S^2 C_O^{\text{ex}} R_{\text{out}} t}{2L_{\text{ex}}^2} \frac{2\sigma}{W} \quad \text{for NRs,} \tag{6}$$

$$E_{\text{ex}}^{\text{tot}} = E_{\text{ex}}^V + E_{\text{ex}}^r = \frac{\mu_O M_S^2 2L_{\text{ex}}^2}{2(R_{\text{out}}^2 - R_{\text{in}}^2)} \ln \frac{R_{\text{out}}}{R_{\text{in}} + 0.5L_{\text{ex}}} + \frac{\mu_O M_S^2 C_O^{\text{ex}} R_{\text{out}} t}{2L_{\text{ex}}^2} \frac{2\sigma}{W} \quad \text{for NDs.} \tag{7}$$

D. Magnetostatic energy

The magnetostatic energy of the system is considered to be an effect of the roughness of the surface and induced only from the outer part (face and side surface). In this case, the energy expression of the roughness contribution term to the magnetostatic energy of the vortex state [19] is given by

$$E_{\text{MS}} = \frac{E_O^{\text{MS}} \xi t}{t + \sigma} \frac{2\sigma}{w} \quad \text{for NRs.} \tag{8}$$

In the case of NDs, the extra magnetostatic energy due to the out-of-plane magnetization at the vortex core, referred to as the vortex-core magnetostatic energy, $E_{\text{MS}}^{\text{VC}}$, is quantitatively calculated by $E_{\text{MS}}^{\text{VC}} = (L_{\text{ex}}/R_{\text{out}})^2$. Thus, the total

magnetostatic energy of NDs, $E_{\mathrm{MS}}^{\mathrm{tot}}$, is

$$E_{\mathrm{MS}} = E_{\mathrm{MS}}^{\mathrm{VC}} + E_{\mathrm{MS}} = \left(\frac{L_{\mathrm{ex}}}{R_{\mathrm{out}}}\right)^2 + \frac{E_o^{\mathrm{MS}}\xi t}{t+\sigma}\frac{2\sigma}{w} \quad \text{for NDs,} \tag{9}$$

where $E_O^{\mathrm{MS}} = 0.36 \pm 0.01$, $\xi = 2\sigma/\lambda$, λ is a roughness correlation length in the order of $\sqrt{2}c$, $c = 5$ nm is the cell size, and $\sigma = \sqrt{2}c/4$ is the roughness amplitude. This empirical equation should describe the edge-roughness effect of magnetic states where the magnetostatic energy term dominates.

IV. RESULTS AND DISCUSSION

Figures 1(a) and 1(b) show a schematic illustration of NRs and NDs, indicating the surface and side charge regions, which are essential for analyzing the energy terms in the magnetic vortex system. The circular region indicated by the black arrows in NDs, Fig. 1(b), is the vortex core, and arrows perpendicular to the plane are responsible for out-of-plane magnetization. Figure 1(c) shows the phase diagram, where the dependence of the magnetic behavior on the geometry (thickness, t, and diameter, d) of the NDs, i.e., the transition from a SD state to a vortex configuration separated by their boundary line, is analyzed through the theoretical model and micromagnetic simulation. In NDs, three possible ground states of magnetization are found at remanence: in-plane SD, vortex, and out-of-plane SD; the point at which the three ground states have the same energy (thickness $t \sim 80$ nm and diameter $d \sim 66$ nm) is called the "triple point". If the NDs are very thin, then all magnetic moments are arranged in plane; if the diameter is small and the thickness is large, then magnetization is perpendicular to the plane of the NDs (out of plane); and another ground state is a vortex state observed above a certain thickness and diameter, which is referred to as the critical size. The phase diagram constructed through the theoretical model is in very good agreement with the micromagnetic simulation result. However, the small discrepancy at the boundary line is probably due to the effect of cubic cell discretization in the micromagnetic simulation, which contributes to the additional roughness energy, and hence, the total ground-state energy

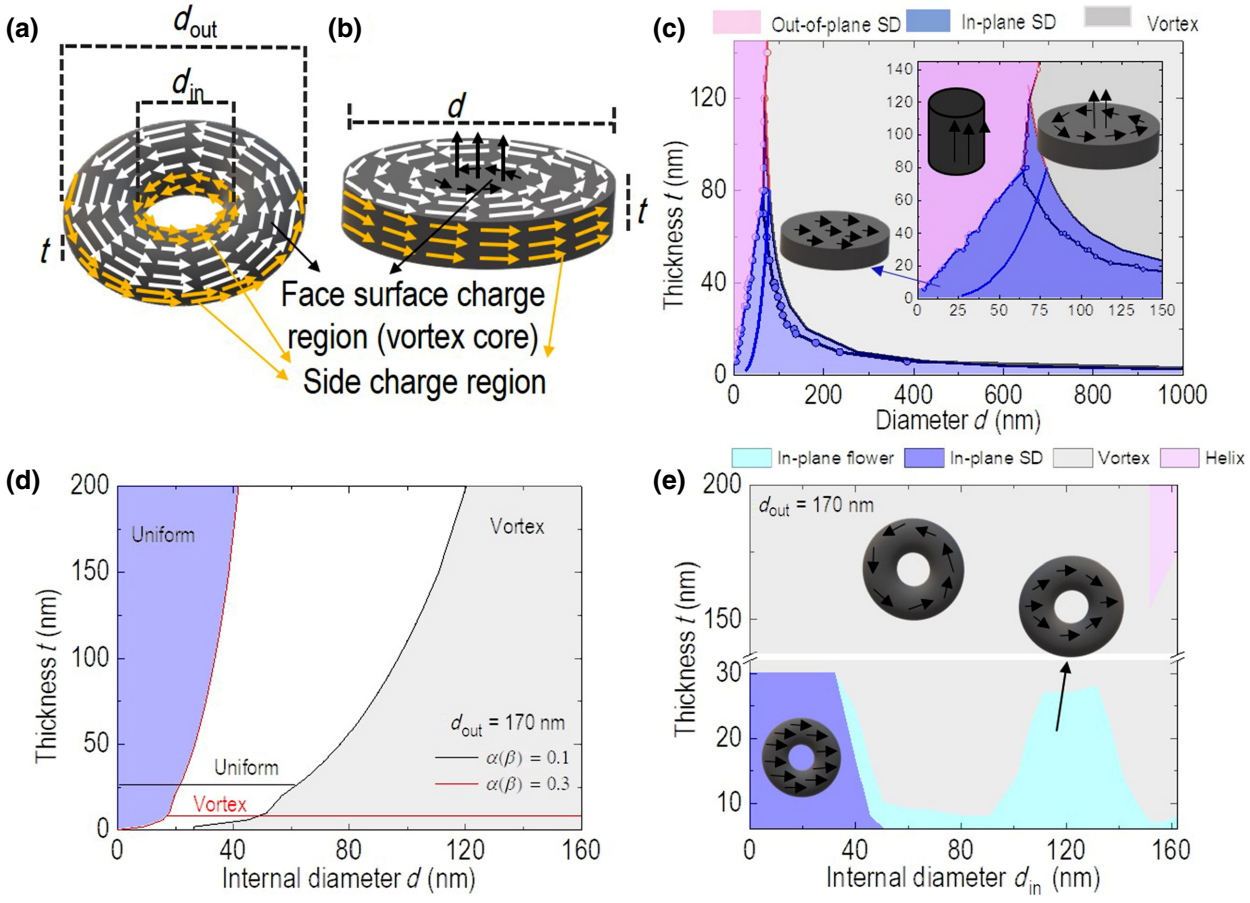

FIG. 1. Schematic pictures of (a) NRs and (b) NDs; (c) phase diagram of NDs obtained from the theoretical model (solid line) and micromagnetic simulation (solid line with circles); and (d),(e) phase diagrams of NRs obtained from the theoretical model and micromagnetic simulation, respectively.

of the system. Such effects are not observed when constructing a phase diagram from the theoretical model. The nature of the phase diagram constructed for NDs, which provides explicit transition lines among vortex and in- and out-of-plane SDs, agrees well with the theoretical and simulated results found elsewhere [24–27].

Figures 1(d) and 1(e) show the theoretical and simulated phase diagrams of NRs as a function of thickness, t, and internal diameter, d_{in}, at a constant outer diameter, d_{out}. The presence of the hole in the ring considerably modifies the vortex state, avoiding the possible out-of-plane SD state. Theoretically, we find only two possible ground states, i.e., the uniform state (SD state) and vortex state. Here, we analyze the minimum-to-maximum region, below $[<\alpha(\beta)=0.1]$ and above $[>\alpha(\beta)=0.3]$, where the possibility of the ground-state vortex configuration is disregarded. In addition, it is worth mentioning that an intermediate mixed-vortex phase could be possible for $0.1<\alpha(\beta)<0.3$ [21]; this phase depends on the inner radius of the NRs and occurs if the inner radius is sufficiently small compared with the outer diameter. Furthermore, within the reported range of t, d_{in}, and d_{out} here, four ground states, namely, in-plane SD, in-plane flower (also called onion), vortex, and helix states, are observed through the micromagnetic simulation and agree well with the literature [28–30], and most of the region is found to correspond to the vortex state at intermediate values of thickness, t, and internal diameter, d_{in}, at fixed d_{out}. We find that the triple point, i.e., the boundary point of in-plane SD, in-plane flower, and vortex in NRs, is close to thickness $t\sim 30$ nm and internal diameter $d_{\text{in}}\sim 37$ nm.

Furthermore, when thickness t approaches a larger value, the demagnetization energy increases proportionally [19], and, when $t>d_{\text{in}}$, the strong out-of-plane demagnetizing field compels the top and bottom in-plane spins to point out and ultimately form a helix state. The helix state is a combination of the vortex and out-of-plane configurations, in which the spins in the top and bottom planes of the NRs exhibit a counterclockwise vortex configuration to reduce the fringe field, while, in the middle planes, the spin is indicated to be out of plane along the z axis [31]. These in-plane flower and helix states are considered to be metastable states that exhibit a nonzero net magnetization, although they have NR structures, leading to considerable magnetostatic interactions in suspensions and aggregation [14,32,33]; therefore, these dimensional NRs are usually not recommended for biomedical applications.

A. Exchange energy

Figure 2(a) shows the exchange energy, E_{ex}, of NDs as a function of diameter, in which E_{ex} is decreasing with increasing diameter (from diameter $d=200$ to 1000 nm), where the solid line and circles indicate the energy obtained from the theoretical model and micromagnetic simulation, respectively. Quantitatively, when the diameter is increased by about 5 times, E_{ex} is decreased by about 16 times; NDs become a more energetically favorable state (lower-energy state) when going far from the critical diameter (approximately 92 nm for Fe_3O_4, not shown here), as observed in Fig. 2(a). Furthermore, from Fig. 2(b), it is observed that E_{ex} in the vortex region is independent of the thickness of the NDs. It is reported that the total energy is almost completely dominated by the exchange energy because of the formation of a central vortex within the vortex state of NDs, whereas the single-domain state is dominated mainly by the demagnetization energy generated by charges on top of the lateral surfaces [34,35]. For large structures, the vortex state lowers the system's energy by decreasing stray fields, and thus, reducing the magnetostatic energy. The central vortex of NDs has a vortex core of a certain radius, the so-called vortex-core radius, r_{VC}, which is much smaller than the radius of the NDs, R ($r_{\text{VC}}\ll R$), and the magnetization in the region is out of plane, $m_z\neq 0$, but much smaller than in-plane magnetization, whereas, in the outer regions of the vortex, magnetization lies completely in plane. In principle, the vortex core is a stable formation, which is greatly coupled with exchange forces, and it can be assumed that dynamic magnetization has significant values just outside of the vortex core, i.e., in-plane magnetization [36].

The value of the vortex-core radius (r_{VC}) can be obtained by minimizing the total magnetic energy (details are given in Refs. [37,38]); r_{VC} proportionally depends on the radius of the NDs (at constant thickness), which favors a large reduction in exchange energy for a larger structure of the disk center at the expense of a low dipolar-energy increase. For biomedical applications, a large vortex core in NDs is essential, which forces the magnetic remanence to be negligible, thereby enhancing the stability of NDs in suspensions. With decreasing disk diameter at a constant thickness, as shown in Fig. 2(a), the relative contribution of the exchange energy for the central vortex increases, which thus increases the overall energy and renders the vortex state as a single-domain state under a critical diameter, d_c (sizes towards 92 nm are not shown here); the largest exchange energy is observed for 200 nm NDs, since this is close to the single-domain region (single-domain $<d_c<$ vortex). The larger the diameter of NDs is, the longer the displacement of the vortex core, which lowers the exchange energy and renders better stability of the vortex state, reducing remanent magnetization. Additionally, it is worth mentioning that, by applying a field (H), the exchange energy decreases with increasing displacement of the vortex(es) [39]. On the other hand, the micromagnetic simulations precisely identify the equilibrium configuration, which is not, essentially, the perfect vortex state. Nevertheless, the discreteness of the method and the utilization of a cubic mesh are sources of

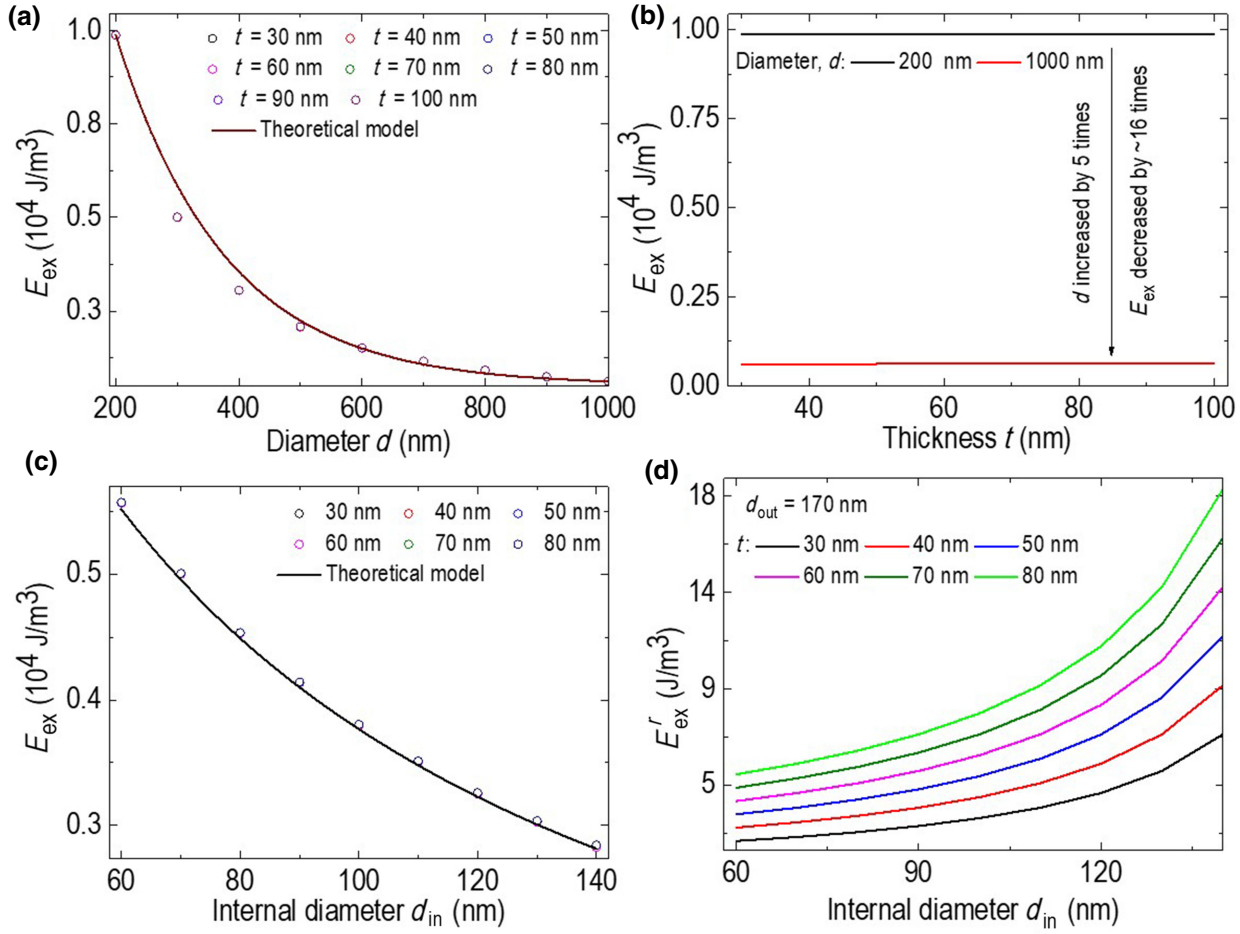

FIG. 2. (a) Exchange energy, E_{ex}, evolution of NDs as a function of diameter, d; (b) comparison of E_{ex} loss with increasing diameter of NDs; and (c),(d) exchange energy, E_{ex}, evolution and roughness contribution to E_{ex} in NRs as a function of internal diameter, d_{in}, respectively.

systematic errors of nonrectangular systems, thus raising the imprecision of micromagnetic simulations because of discretization [35]. This is more applicable to NDs and NRs, since the circular boundary is estimated by a staircase of straight-line segments. Such edge roughness causes surface charges that raise the demagnetization energy. To investigate such roughness energies analytically, a simple analytical method is derived by taking into account the ratio of the perimeter to the volume of the nanoparticles [Eq. (3)]; the roughness-energy contribution is generated from the edge of dimension-based nanoparticles. An increase in thickness contributes to the additional energy, the so-called "exchange-roughness energy", from the edge surface of each disk, which acts to make the edge spins point in directions far from the azimuthal direction. Figure S1 within the Supplemental Material [40] shows the linear dependency of the exchange-roughness energy (E^r_{ex}) with thickness, t. Although it is negligible compared with E_{ex}, its effect is accountable within the intermediate region (200–500 nm) due to some significant energy discrepancies between the theoretical model and micromagnetic simulations. We note that E^r_{ex} is significant close to the single domain, but it dominates when NDs are far from the SD region, even though the small exchange-roughness energy of the particles examined could contribute significantly to the magnetic behavior of a disk-shaped particle in the prevortex stadium [15]. With the edge roughness being taken into account analytically, the total exchange energy leads to good agreement between the theoretical model and simulations, as shown in Fig. 2(a).

We note that the geometry of a ring is a disk when considering the internal diameter to be $d_{in}=0$, and it has already been mentioned that, in such cases, $m_z \neq 0$. The maximum vortex-core magnetization amplitude is one (for a disk) and the minimum is zero (for a narrow ring, $d_{in}/d_{out} > 0.9$). This means that the amplitude of the vortex core, m_z, varies from one to zero in rings, depending on the width, w ($w = d_{out} - d_{in}$, where d_{out} is the external diameter); a wider ring has greater m_z. Figure 2(c) shows

E_{ex} in NRs as a function of internal diameter, d_{in}, at a constant thickness, t, and reveals a similar energy trend to that exhibited by NDs. E_{ex} decreases with increasing d_{in}, where the solid line and circles indicate the energy obtained by the theoretical model and micromagnetic simulation, respectively, which are consistent with each other. The formation of the vortex core at a wider ring (closer to a disk) is expected; however, m_z is <1 and is responsible for the generation of the exchange energy. When the width of the ring decreases, the formation of the core has a lower probability and cannot be expected for narrow rings ($d_{in}/d_{out} > 0.9$), and the contribution to the exchange energy decreases with increasing internal diameter, d_{in}. Likewise, for NDs, Fig. 2(d) shows the additional roughness energy, E^r_{ex}, contribution to E_{ex} as a function of d_{in}. The increase in E^r_{ex} with increasing d_{in} is due to the increased perimeter of the inner side of the ring, which contributes to making the inner edge spins point in directions away from the azimuthal direction. Furthermore, E^r_{ex} is linearly dependent on the thickness of the NRs, as shown in Fig. S2 within the Supplemental Material [40]. The E^r_{ex} contribution to E_{ex} in NRs as a function of thickness is 1 order of magnitude greater than that in NDs within approximately similar dimensions (NDs, $d = 200$ nm, $t = 40$ nm; NRs, $d_{out} = 170$ nm, $d_{in} = 140$ nm, and $t = 40$ nm). This larger contribution arises from the inner edge of the NRs.

B. Magnetostatic energy

The magnetostatic energy of the system is considered to be an effect of the roughness of the surface. This roughness is the source of the distributed magnetostatic charges on top of the interfaces. In practice, edge roughness arises due to different steps involved during the synthesis process, for instance, nanoparticles fabricated by different deposition techniques and thermal treatments [41] and with different substrates [42], growth conditions [43], growth rates [44], and nanoparticle thicknesses [45,46]. This edge roughness makes a significant contribution to the nucleation field for magnetization reversal [47–49] and, more importantly, to the stabilization of metastable equilibrium states [50]. Unlike the small roughness-energy contribution to the exchange energy, as discussed above, the edge roughness causes and increased magnetostatic energy contribution, depending on the geometry of the nanoparticles. The magnetostatic energy consists of significant surface (on the faces and sides) and negligible volume (for small thickness) contributions [34]. In the case of disk-shaped particles, two active inhomogeneous terms appear: (a) a face-surface charge term (easy-plane anisotropy of thin disks and easy-axis anisotropy of thick disks), which can change sign near the edge; and (b) an edge-side charge term, which causes the tangential magnetization distribution, producing clockwise or counterclockwise vortex chirality [51,52]. The vortex core generates nonvanishing surface magnetostatic charges with different signs on top of the different face surfaces. Their minimization causes complicated vortex results both in the plane and in the axial direction [53]. An inhomogeneous magnetization arrangement in magnetically soft nanoparticles is due to the stray field produced by surface magnetostatic charges. The core magnetostatic energy is only produced by the surface magnetic charges along the perimeter of the particle, since volume charges are absent (div $m = 0$) and thickness t remains unchanged with the vortex displacement. The vortex-core magnetostatic energy in disks arises from the out-of-plane magnetization ($m_z \neq 0$); surface magnetic charges on top of the faces of the disk localize near the vortex center, which is a topological singularity. On the top and bottom surfaces, the surface charges are proportional to m_z, and the net side-surface charge is zero on the circumference of the disk [54]. Thus, $E^{VC}_{MS} = (L_{ex}/R_{out})^2$, where a vortex-core radius approximately equal to L_{ex} is used, in agreement with micromagnetic simulations [19,55].

Figures 3(a) and 3(b) show the vortex core and roughness magnetostatic energy profiles as a function of diameter d in disks; the E^{VC}_{MS} contribution to the total magnetostatic energy is almost zero (approximately 10^5 times lower); thus, the total magnetostatic energy is dominated by E^r_{MS}. Mathematically, it seems that the magnetostatic energy is inversely proportional to the square of the disk diameter, d, and directly proportional to the thickness, t (see Fig. S3 within the Supplemental Material [40]); however, the physics of the magnetic vortex system and the interpretation are quite different. At remanence (zero applied field, $H = 0$), the centers of the vortices are at the centers of the NDs. In this state, the magnetic charges are practically absent, and the magnetostatic interaction between the individual NDs is small. Once an external magnetic field is generated and applied to the system, the centers of the vortices are shifted, and few magnetic charges arise at the boundaries of the NDs, which leads to an increase in the self-magnetostatic energy of the poles distributed on both faces of the disks with surface density $\sigma(\rho)$ [37]. The total displacement of the vortex core from the center to the edge boundary is an important determining factor in reducing the core magnetostatic energy, depending on the diameter of the NDs. When the vortex core increases the circumference of NDs, the elliptically distorted vortex shape effectively reduces the core magnetostatic energy because of the reduction in surface charge. The influence of vortex distortion is then crucially important for NDs with a smaller diameter (near the critical diameter discussed above), since the vortex core occupies approximately all the disk volume. When the applied field is sufficient to annihilate the vortex state, the minimum total energy reaches a maximum, making the vortex state unstable; as the vortex core is close to the edge, the surface charge density induced by the magnetic charges on the top and bottom faces increases on the circumference.

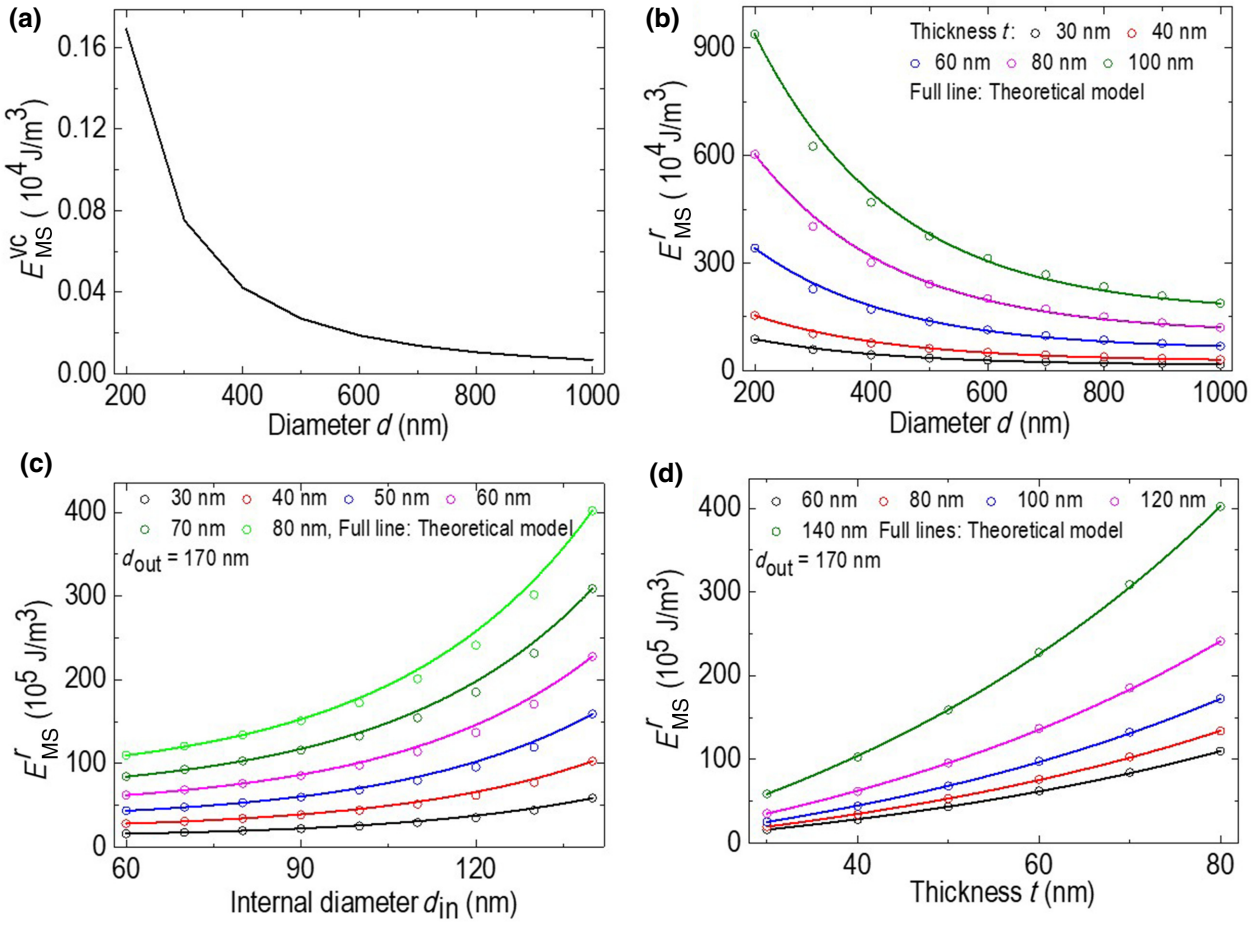

FIG. 3. (a) Vortex-core magnetostatic energy density, E^{VC}_{MS}, evolution of NDs as a function of diameter, d; (b) magnetostatic energy, E^{r}_{MS}, evolution as a function of diameter, d, in NDs; and (c),(d) magnetostatic energy, E^{r}_{MS}, evolution as a function of internal diameter, d_{in}, and thickness, t, in NRs, respectively.

Accordingly, the systems proceed towards the next energy minimum, which can be found for the state with a homogeneous magnetization distribution. On the other hand, the vortex state can be stabilized by the dominant energy engendered by magnetic charges on the side (thickness) of the NDs, i.e., the roughness magnetostatic energy. The rate of the decrease in this energy decreases with increased diameter, d, at a fixed thickness, t. This decreased rate is related to the decrease in the possible amount of side magnetic charges forming at $t < d$ with increasing d at fixed t [34].

Similarly, Figs. 3(c) and 3(d) show the magnetostatic energy profile of NRs as a function of thickness, t, and internal diameter, d_{in}, at constant external diameter, d_{out}. An increase in the internal diameter increases the perimeter of the inner side of NRs, and thus, more side charge can contribute to the magnetostatic energy, E^{r}_{MS}. Likewise, side charges are increased with an increase in thickness, contributing more to E^{r}_{MS}. The absence of the core region is a great advantage of nanorings over disks that avoids possible remanent magnetization, i.e., no out-of-plane magnetization ($m_z = 0$), and hence, enhances the stability of NRs. Therefore, the total roughness magnetostatic energy induced by side charges is considered to be the total magnetostatic energy in NRs.

In the above section, we comprehensively study the roles of the shape, size, vortex core, magnetic surface, side charges, holes, and cell discretization or additional roughness contributions in the evolution of the exchange and magnetostatic energies of NDs and NRs through a theoretical model and micromagnetic simulations. Taking all these physical factors together, we have an idea of how they affect the stabilization and agglomeration of vortex NDs and NRs and the advantage of NRs over NDs. Considering the potential to be used in cancer-cell destruction, we further take NDs and NRs with different d_{in} at fixed $t = 50$ nm and $d_{out} = 170$ nm (diameter, d, considering d_{out} for NDs to obtain a common diameter with NRs). The reasons for using this size range for further study are as follows: (a) this size range can be synthesized and (b) it

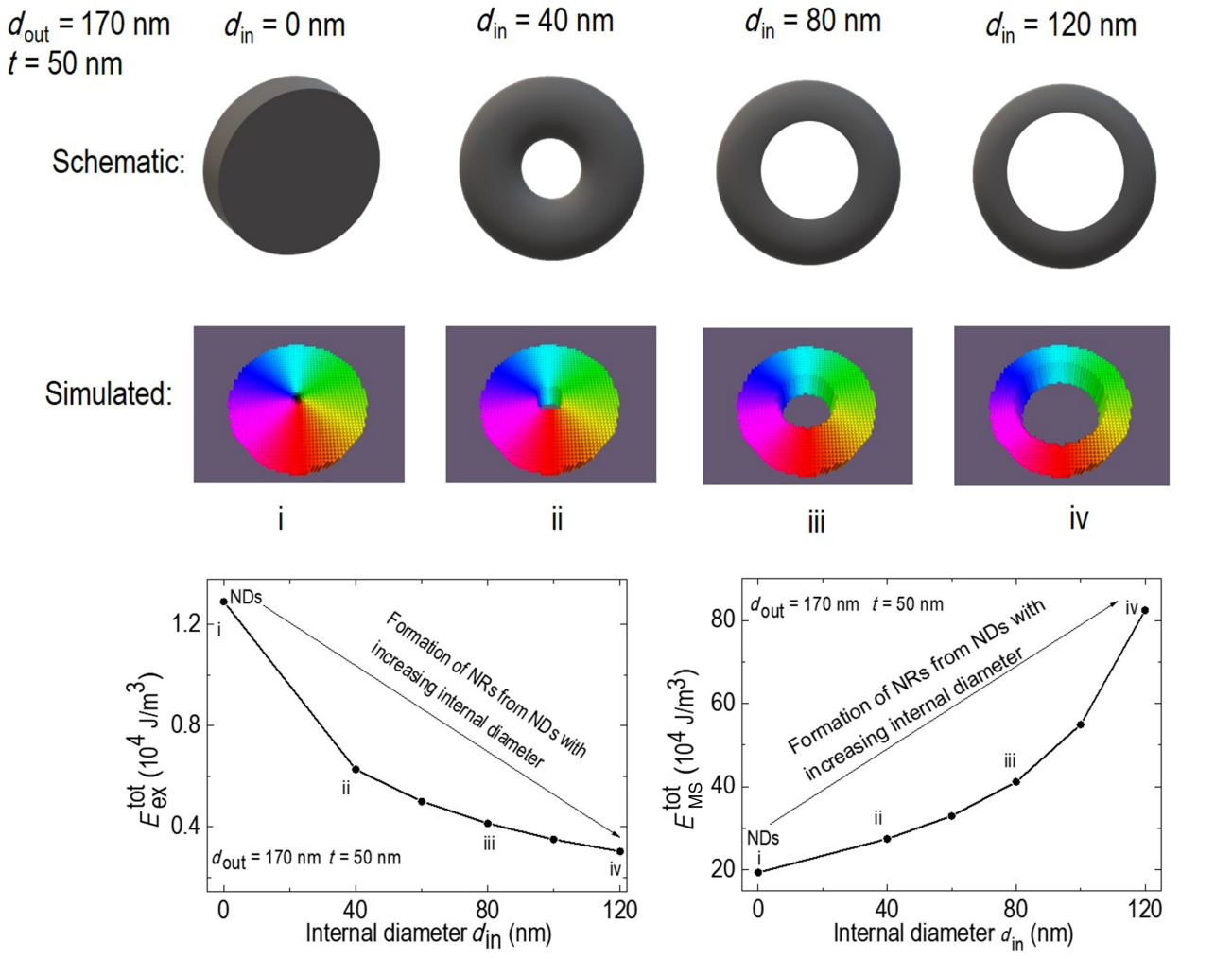

FIG. 4. (a) Schematic geometrical formation of NRs from NDs; (b) simulated spin configuration for each geometry in the vortex state ($H = 0$); and (c),(d) total exchange energy, E_{ex}^{tot}, and total magnetostatic energy, E_{MS}^{tot}, evolution from NDs to NRs as a function of d_{in} at fixed $t = 50$ nm and $d_{out} = 170$ nm. We assume $d_{in} = 0$ nm for NDs.

is within that for biological consideration for injection into living cells [12,13,17].

Figures 4(a) and 4(b) show schematics and vortex-state spin configurations of NDs and NRs with increasing d_{in}. The exchange and magnetostatic energies of the respective geometries (NDs and NRs) are shown in Figs. 4(c) and 4(d). We discuss above how the energy evolves on NDs and NRs separately. The energy evolution from the starting NDs into NRs shown in Figs. 4(c) and 4(d) demonstrates that the total exchange energy, E_{ex}^{tot}, is reduced by more than half along the corresponding steps (i)–(iv) [Fig. 4(b)]. This loss of energy is due to loss of the vortex core, since the vortex core is responsible for the overall exchange energy in the vortex state of NDs, as discussed above. This means that the vortex state in NRs definitely exists in a much lower energetically favorable state than that in NDs, and hence, becomes more stable. Similarly, the increase in total magnetostatic energy, E_{MS}^{tot}, with increasing d_{in} is due to the inner-edge-perimeter (depending on hole formation) contribution in the single-domain state. Here, E_{ex}^{tot} and E_{MS}^{tot} represent the total exchange energy (exchange energy, E_{ex}, plus additional roughness energy, E_{ex}^{r}) and total magnetostatic energy (vortex-core magnetostatic energy, E_{MS}^{VC}, plus roughness energy, E_{MS}^{r}).

C. Dispersion and agglomeration capability

For most biomedical uses of magnetic nanoparticles, the samples are in colloidal form, and thus, obtaining stable particle dispersions and avoiding subsequent agglomeration is a primary concern. The magnetic vortex configurations for NDs and NRs discussed above show negligible remanence values in the absence of an applied field, favoring stable dispersions without agglomeration in a liquid medium, if their reversible magnetic behavior at low fields is preserved, as demonstrated in previous

experimental work reported elsewhere [11–13,17,30]. The physical parameters that determine reversible magnetic behavior can be optimized through the numerical analysis presented here by reducing the susceptibility of the nanosystems. In recent work, Leulmi *et al.* [56] proposed two kinds of theoretical concepts for magnetic susceptibilities, the actual susceptibility of particles, $\chi(0)$, and the critical susceptibility (χ_{critical}), also called the threshold susceptibility, below which self-polarization of particles can be avoided. Such magnetic susceptibilities are given as

$$\chi(0) = \frac{4\pi}{2\pi\left[\ln\left(\frac{8}{\beta}\right) - \frac{1}{2}\right]},$$

$$\chi_{\text{critical}} = \frac{\partial M}{\partial H} = \frac{16K}{\left[\sum_{k=1}^{N}(1/k^3)\right]\beta}.$$

The sum, in which N refers to the number of particles, converges quickly to 1.202, so a larger value of N has minimal importance. The numerical constant K, in the order of one to four, refers to the stray field generated on a particle. In the present case, we assume $\beta = t/(R_{\text{out}} - R_{\text{in}})$ as the aspect ratio.

Figure 5(a) shows the actual susceptibility, $\chi(0)$, and critical susceptibility, χ_{critical}, of NDs and NRs as a function of internal diameter. Here, $d_{\text{in}} = 0$ refers to NDs. The magnetic susceptibility decreases with increasing d_{in} (hole) from NDs to NRs at constant $d_{\text{out}} = 170$ nm and $t = 50$ nm. The value of $\chi(0)$ is lower than the critical self-polarization value (χ_{critical}), even at $K = 1$, which indicates that the sizes of NDs and NRs we take here are free from the generation of a stray field. In addition, the obtained result of $\chi(0) < \chi_{\text{critical}}$ provides strong evidence for vortex nanoparticles avoiding agglomeration or at least reduced agglomeration [56]. Compared with NDs, NRs have a lower $\chi(0)$, which suggests better dispersion and stabilization in a suspension. The lower value of $\chi(0)$ in NRs is due to the absence of a vortex core, which has significant out-of-plane magnetization and contributes to the exchange energy in the case of NDs; details of the vortex-core and hole contributions to the energy evolution in NDs and NRs have already been discussed above. Furthermore, our concern is how the vortex core and hole can affect the remanent magnetization of these systems. Figure 5(b) shows the micromagnetic simulated hysteresis loop for NRs and NDs at a specific size. It is observed that about

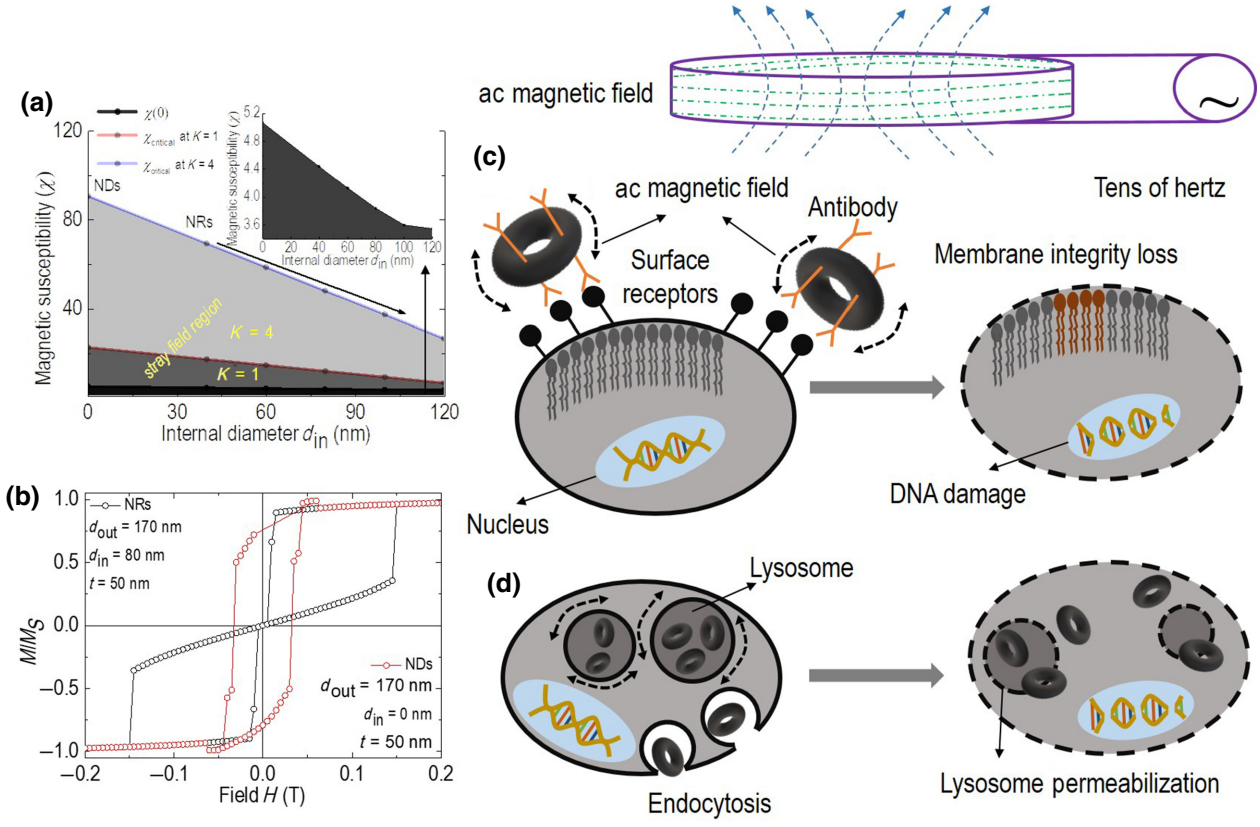

FIG. 5. (a) Actual susceptibility, $\chi(0)$, and critical susceptibility, χ_{critical}, from NDs to NRs as a function of internal diameter d_{in}; (b) micromagnetic simulation of NDs and NRs at a defined size; and (c),(d) illustration of extracellular and intracellular magnetomechanical actuation of vortex NRs on cancer cells, respectively; these schematics are made by ourselves, but are inspired by Ref. [11].

75% of the saturation magnetization remains as remanence in NDs, although a flux-closure vortex configuration is observed, whereas zero remanence is observed in NRs. The simulation results agree well with the reported experimental values for similar NDs [12,13] and NRs [17,57]. Thus, Figs. 5(a) and 5(b) collectively confirm the roles of the vortex core and hole in the magnetic susceptibility and remanence properties in a vortex nanosystem. The hollow nature of the NRs changes the topological properties of the vortex solution, making it unnecessary for the vortex amplitude to attain a value of unity at the center of the ring. The NR does not exhibit an out-of-plane magnetization component at all if the inner hole is large enough; the amplitude of the vortex decays faster when the inner hole becomes larger, rendering better stabilization or dispersion in suspensions. Figure 5(c) illustrates the extracellular actuation of NRs on cancer cells in which the oscillation of NRs, attached by antibody-receptor bonding, influences the membrane integrity during exposure to ac magnetic field, triggering apoptosis within the cancer cell. Similarly, Fig. 5(d) shows the intracellular actuation of NRs endocytosed within the cancer cell and accumulated in lysosomes, which are permeabilized due to oscillation of the NRs under the influence of ac magnetic field, generating cell self-destruction by apoptosis.

D. Magnetomechanical properties

The biomedical application aimed at targeted cancer-cell destruction and the magnetomechanical vibration efficiency of these NDs and NRs, activated by an alternating field, are thoroughly studied. For the potential case of triggering cancer-cell apoptosis [11], generally, a larger torque applied on the cell membrane is a more efficient treatment. The magnetic torque (τ) acting on a magnetic nanoparticle can be approximated by $\tau = |\mu||B|$, where μ is the magnetic moment and $B = \mu_O H$ represents the magnetic field. Detailed calculations are given in the Supplemental Material [40]. In principle, the initial torque of the nanosystem will be similar, regardless of if the applied magnetic field is rotational. However, a further increase of the field alters the response of the system. In the vortex nanosystem, once the in-plane magnetization of the particles aligns with the plane of the rotating field, magnetization shall rotate, regardless of exerting further torque on the particles [9]. When the applied field (H) is sufficient to saturate nanoparticles, magnetization will align with the field direction; however, as the field approaches zero, nanoparticles will demagnetize and relax in the fluid, returning back to an arbitrary orientation. Similarly, when the magnetic field approaches a maximum, net magnetization is induced in nanoparticles, which tend to align along the field direction. The repetition of this process would cause a continuous oscillation of the nanoparticles.

Figure 6(a) shows the torque exerted for the investigated vortex NDs and NRs. The torque exerted by NDs is higher than that exerted by NRs, as expected, because it depends on the volume; the presence of a hole in the NRs obviously lowers the net volume. An increase in the internal diameter decreases the volume, and thus, decreases the torque. Figure 6(b) shows the upper limit of the force applied to a cell at the edges of NDs and NRs, which can be achieved in the quasistatic regime using material and field parameters during an experiment. The increase in the upper force with increasing internal diameter is due to the additional increase in the inner-edge perimeter along with the external edge. Here, we find that the magnetic-vortex-induced forces are in the range of >100 s of pN. While physically rupturing a cell within a membrane usually requires a minimum of hundreds of pN, it has been demonstrated that even 0.5 pN activates ion channels that could accelerate cell apoptosis [58–60]. Therefore, the investigated NDs and NRs could potentially be used for magnetomechanical cell destruction. The resulting force to oppose the magnetic torque (τ) is almost 3 orders of magnitude greater than the force required to activate an ion channel in the cell membrane. Although NDs can exert a torque (τ) of up to an order of magnitude greater than that of the studied NRs, the NDs have great susceptibility and remanence, as shown in Figs. 6 (a) and (b), which might induce potential agglomeration in suspensions. On the other hand, vortex NRs have lower susceptibility and negligible remanence compared with NDs, which suggests that NRs could be better candidates from a biological perspective. Recently, the effectiveness of cell death or damage in different systems, (a) the perpendicular synthetic antiferromagnetic state (PSAF system) and (b) the vortex state, has been studied to account for the importance of the symmetry of magnetic anisotropy in the PSAF system [9]. This is not the case, nonetheless, in our system, since we are presenting Fe_3O_4 in two different geometries (NRs and NDs) under the same vortex system. Thus, the effectiveness of mechanical cell death depends upon the magnitude of torque and its translation into a force rather than symmetric anisotropy. The torque (τ) of NRs can be enhanced by increasing the thickness, diameter, and applied field (H), since torque does not rely on the material's magnetic properties, such as exchange-stiffness constant. Figure 6(c) clearly shows the linear field-dependent torque exerted by NRs. The idea is to compare the applied field, H, required for NRs to exert a torque (τ) equivalent to that exerted by NDs. Figure 6(d) shows a comparative study of the torque (τ) and required force (F) at the edges of NDs and NRs. In the present case, it is clear that the same torque (τ) as NDs is exerted by NRs with an increase in the applied field of 20%. Similar to Fig. 6(b), the inset of Fig. 6(d) shows the comparative force to be applied to rupture a cell membrane at the edge of NDs and NRs.

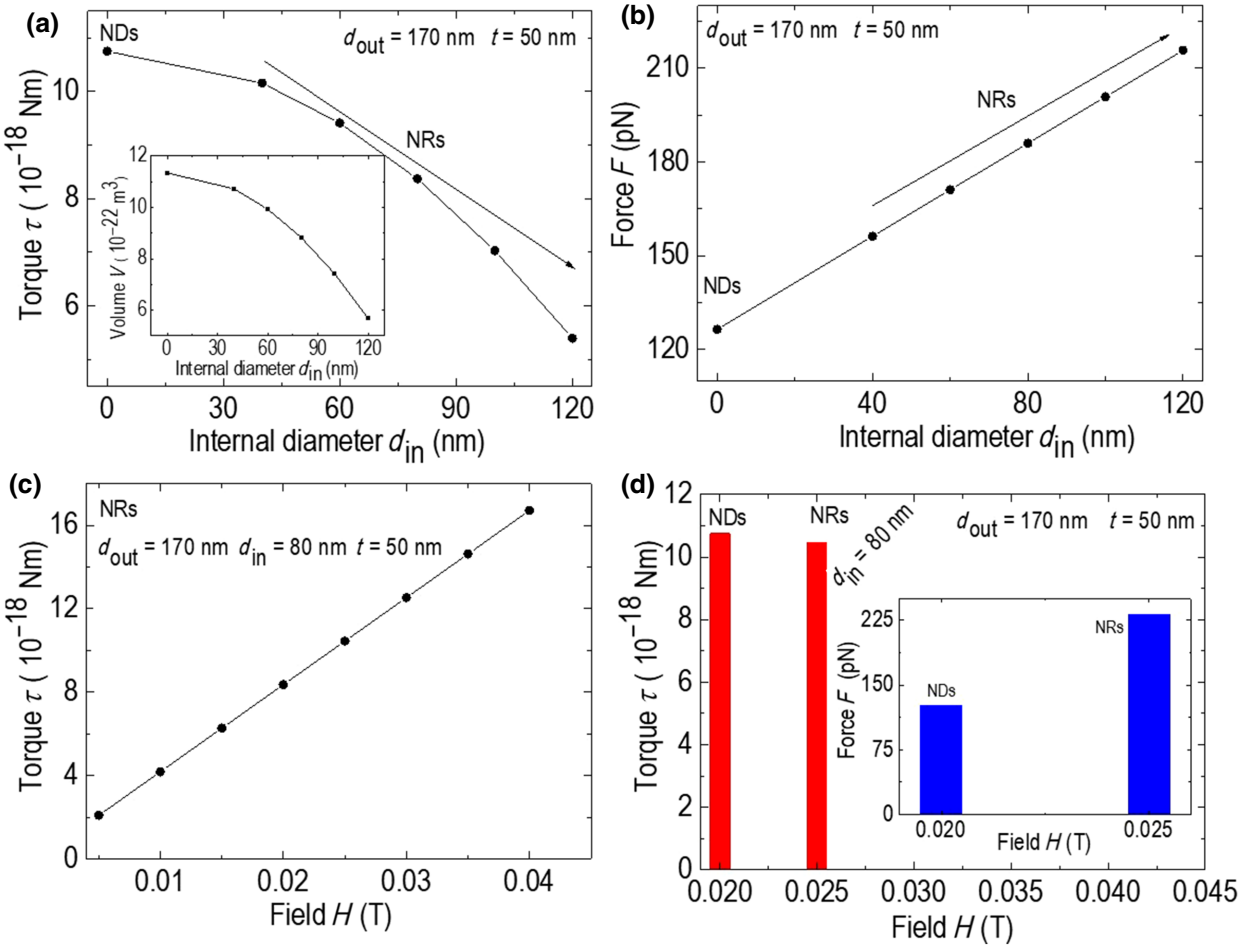

FIG. 6. Torque exerted by NDs and NRs at a defined size; (b) force to be applied to rupture a cell membrane at the edge of NDs and NRs; (c) torque exerted by NRs as a function of applied field, H; and (d) comparative study of torque (τ) and required force (F) at the edge of NDs and NRs at different fields.

Experimentally, a state-of-the-art concept of magnetic-vortex-driven triggering of cancer-cell apoptosis and further death via a magnetomechanical approach was proposed by Kim *et al.* [11] for gold-coated permalloy ($Ni_{20}Fe_{80}$) microdisks with a diameter of 1 μm and a thickness of 60 nm. Later, a few studies expanded on this concept using a magnetic vortex disk as a magnetomechanical transducer to eradicate cancer cells [9,26,56,61]; however, no further theoretical study has been performed by taking vortex rings as a transducer. Recently, Gregurec *et al.* [12] studied Fe_3O_4 vortex NDs (diameter range, 98–226 nm; thickness range, 24–37 nm) as magnetomechanical transducers of signals to remotely control mechanosensory cells under low and slow magnetic fields ($H = 0.026$ T, $f = 5$ Hz). The torque (τ) generated by 226-nm NDs is approximately 1.6×10^{-17} Nm (slightly larger than that of our NDs), and the force to be applied to rupture a cell membrane is approximately 140 pN (larger than that of our NDs but smaller than that of our NRs). Furthermore, they observed that dorsal root ganglia explants contain sensory neurons with an extensive range of mechanoreceptors, and cultures adorned with 226-nm magnetic nanodisks (MNDs) under 0.026 T, 5 Hz, magnetic fields (MFs) did not cause significant and measurable variations in cell viability, indicating that the modest reactions to MFs of hippocampal neurons adorned with 226-nm MNDs were likely to be dominated by the influence of the torque anion-channel gating being greater than that of membrane permeability. Although excellent biological results were obtained by their study with 226-nm NDs, we propose better results for NRs, taking advantage of their negligible remanence and better stability in suspensions. It is necessary to functionalize the nanoparticles with biocompatible materials, so it is suggested to biofunctionalize these vortex NRs before starting to work on cells and inserting them into targeted tumors [2–4,32,42]. Thus, based on the theoretical overview of the energy profile, dispersion or agglomeration capability, torque (τ) exerted, and force applied to oppose the exerted magnetic torque (τ) of vortex NDs and NRs with tuning

of the shape, size, and applied field reported here, we encourage researchers to carry out *in vitro* and *in vivo* experiments using NRs as a cancer-cell transducer to make progress in this emerging research field.

V. CONCLUSIONS

We study the energy evolution, magnetic susceptibility, and magnetomechanical properties of Fe_3O_4 NRs and NDs through theoretical and micromagnetic simulations. The presence of holes in NRs in comparison to NDs significantly reduces the exchange energy and magnetic susceptibility, and hence, minimizes possible agglomeration effects in colloidal dispersions. Our numerical results show that, for constant values of outer diameter, thickness, and applied-field amplitude, the vortex magnetic configuration within ND topologies should be more efficient than the corresponding NR topology in transducing magnetic coupling into mechanical actuation (i.e., physical oscillation of the NDs affecting the membrane integrity). Although vortex NDs could generate larger torque (τ) than vortex NRs, it is important to note that the remanence resulting from the out-of-plane magnetization in the ND vortex core would promote some degree of agglomeration, limiting the use of NDs in actual biological treatments. Possible alternatives to improve the torque of NRs, and therefore, their mechanical effects on biological systems could be to increase either the NR radius (since the magnetic torque depends on the volume) or to work under larger magnetic field amplitudes.

ACKNOWLEDGMENTS

G.N. is grateful to the Brazilian funding agency CAPES and PPGF-UFMA for providing a doctorate fellowship. S.K.S. is grateful to PPGF-UFMA for support in this project. J.A.H.C. thanks CNPq and FAPDF for financial support. J.C.D. thanks ANID/Fondecyt Grant No. 1200782 for financial support. G.F.G. acknowledges partial financial support from the Spanish Ministerio de Ciencia, Innovación y Universidades (Project No. PID2019-106947RB-C21).

[1] Y. Gao, J. Lim, S. H. Teoh, and C. Xu, Emerging translational research on magnetic nanoparticles for regenerative medicine, Chem. Soc. Rev. **44**, 6306 (2015).

[2] O. L. Gobbo, K. Sjaastad, M. W. Radomski, Y. Volkov, and A. Prina-Mello, Magnetic nanoparticles in cancer theranostics, Theranostics **5**, 1249 (2015).

[3] Z. R. Stephen, F. M. Kievit, and M. Zhang, Magnetite nanoparticles for medical MR imaging, Mater. Today **14**, 330 (2011).

[4] Y. Cheng, R. A. Morshed, B. Auffinger, A. L. Tobias, and M. S. Lesniak, Multifunctional nanoparticles for brain tumor imaging and therapy, Adv. Drug Deliv. Rev. **66**, 42 (2014).

[5] M. Goiriena-Goikoetxea, D. Muñoz, I. Orue, M. L. Fernández-Gubieda, J. Bokor, A. Muela, and A. García-Arribas, Disk-shaped magnetic particles for cancer therapy, Appl. Phys. Rev. **7**, 011306 (2020).

[6] G. Niraula, J. A. H. Coaquira, F. H. Aragon, A. F. Bakuzis, B. M. G. Villar, F. Garcia, D. Muraca, G. Zoppellaro, A. I. Ayesh, and S. K. Sharma, Stoichiometry and Orientation- and Shape-Mediated Switching Field Enhancement of the Heating Properties of Fe_3O_4 Circular Nanodiscs, Phys. Rev. Appl. **15**, 014056 (2021).

[7] R. J. Mannix, S. Kumar, F. Cassiola, M. Montoya-Zavala, E. Feinstein, M. Prentiss, and D. E. Ingber, Nanomagnetic actuation of receptor-mediated signal transduction, Nat. Nanotechnol. **3**, 36 (2008).

[8] M. Chen, J. Wu, P. Ning, J. Wang, Z. Ma, L. Huang, G. R. Plaza, Y. Shen, C. Xu, Y. Han, M. S. Lesniak, Z. Liu, and Y. Cheng, Remote control of mechanical forces via mitochondrial-targeted magnetic nanospinners for efficient cancer treatment, Small **16**, 1905424 (2020).

[9] R. Mansell, T. Vemulkar, D. C. M. C. Petit, Y. Cheng, J. Murphy, M. S. Lesniak, and R. P. Cowburn, Magnetic particles with perpendicular anisotropy for mechanical cancer cell destruction, Sci. Rep. **7**, 1 (2017).

[10] S. Leulmi, X. Chauchet, M. Morcrette, G. Ortiz, H. Joisten, P. Sabon, T. Livache, Y. Hou, M. Carrière, S. Lequien, and B. Dieny, Triggering the apoptosis of targeted human renal cancer cells by the vibration of anisotropic magnetic particles attached to the cell membrane, Nanoscale **7**, 15904 (2015).

[11] D.-H. Kim, E. A. Rozhkova, I. V. Ulasov, S. D. Bader, T. Rajh, M. S. Lesniak, and V. Novosad, Biofunctionalized magnetic-vortex microdiscs for targeted cancer-cell destruction, Nat. Mater. **9**, 165 (2010).

[12] D. Gregurec, A. W. Senko, A. Chuvilin, P. D. Reddy, A. Sankararaman, D. Rosenfeld, P. H. Chiang, F. Garcia, I. Tafel, G. Varnavides, E. Ciocan, and P. Anikeeva, Magnetic vortex nanodiscs enable remote magnetomechanical neural stimulation, ACS Nano **14**, 8036 (2020).

[13] Y. Yang, X. Liu, Y. Lv, T. S. Herng, X. Xu, W. Xia, T. Zhang, J. Fang, W. Xiao, and J. Ding, Orientation mediated enhancement on magnetic hyperthermia of Fe_3O_4 nanodisc, Adv. Funct. Mater. **25**, 812 (2015).

[14] S. P. Li, D. Peyrade, M. Natali, A. Lebib, Y. Chen, U. Ebels, L. D. Buda, and K. Ounadjela, Flux Closure Structures in Cobalt Rings, Phys. Rev. Lett. **86**, 1102 (2001).

[15] M. Rahm, M. Schneider, J. Biberger, R. Pulwey, J. Zweck, D. Weiss, and V. Umansky, Vortex nucleation in submicrometer ferromagnetic disks, Appl. Phys. Lett. **82**, 4110 (2003).

[16] C. A. Ross, M. Hwang, M. Shima, J. Y. Cheng, M. Farhoud, T. A. Savas, H. I. Smith, W. Schwarzacher, F. M. Ross, M. Redjdal, and F. B. Humphrey, Micromagnetic behavior of electrodeposited cylinder arrays, Phys. Rev. B: Condens. Matter Mater. Phys. **65**, 12 (2002).

[17] X. L. Liu, Y. Yang, C. T. Ng, L. Y. Zhao, Y. Zhang, B. H. Bay, H. M. Fan, and J. Ding, Magnetic vortex nanorings: A New class of hyperthermia agent for highly efficient In vivo regression of tumors, Adv. Mater. **27**, 1939 (2015).

[18] R. D. McMichael and B. B. Maranville, Edge saturation fields and dynamic edge modes in ideal and nonideal

magnetic film edges, Phys. Rev. B: Condens. Matter Mater. Phys. **74**, 024424 (2006).

[19] C. A. F. Vaz, C. Athanasiou, J. A. C. Bland, and G. Rowlands, Energetics of magnetic ring and disk elements: Uniform versus vortex state, Phys. Rev. B: Condens. Matter Mater. Phys. **73**, 054411 (2006).

[20] D. R. Altbir Drullinsky, J. E. Escrig Murua, E. O. Kamenetskii, and P. M. Landeros Silva, *Electromagnetic, Magnetostatic, and Exchange-Interaction Vortices in Confined Magnetic Structures* (Transworld Research Network, Kerala, India, 2008).

[21] P. Landeros, O. J. Suarez, A. Cuchillo, and P. Vargas, Equilibrium states and vortex domain wall nucleation in ferromagnetic nanotubes, Phys. Rev. B: Condens. Matter Mater. Phys. **79**, 024404 (2009).

[22] J. Escrig, P. Landeros, D. Altbir, E. E. Vogel, and P. Vargas, Phase diagrams of magnetic nanotubes, J. Magn. Magn. Mater. **308**, 233 (2007).

[23] H. Hoffmann and F. Steinbauer, Single domain and vortex state in ferromagnetic circular nanodots, J. Appl. Phys. **92**, 5463 (2002).

[24] J. d'Albuquerque e Castro, D. Altbir, J. C. Retamal, and P. Vargas, Scaling Approach to the Magnetic Phase Diagram of Nanosized Systems, Phys. Rev. Lett. **88**, 2372021 (2002).

[25] F. Porrati and M. Huth, Diagram of the states in arrays of iron nanocylinders, Appl. Phys. Lett. **85**, 3157 (2004).

[26] M. Goiriena-Goikoetxea, A. García-Arribas, M. Rouco, A. V. Svalov, and J. M. Barandiaran, High-yield fabrication of 60 nm permalloy nanodiscs in well-defined magnetic vortex state for biomedical applications, Nanotechnology **27**, 175302 (2016).

[27] S. H. Chung, R. D. McMichael, D. T. Pierce, and J. Unguris, Phase diagram of magnetic nanodisks measured by scanning electron microscopy with polarization analysis, Phys. Rev. B: Condens. Matter Mater. Phys. **81**, 024410 (2010).

[28] F. Montoncello, L. Giovannini, F. Nizzoli, H. Tanigawa, T. Ono, G. Gubbiotti, M. Madami, S. Tacchi, and G. Carlotti, Magnetization reversal and soft modes in nanorings: Transitions between onion and vortex states studied by brillouin light scattering, Phys. Rev. B: Condens. Matter Mater. Phys. **78**, 104421 (2008).

[29] P. Landeros, J. Escrig, D. Altbir, M. Bahiana, and J. D'Albuquerque e Castro, Stability of magnetic configurations in nanorings, J. Appl. Phys. **100**, 044311 (2006).

[30] Y. Yang, X. L. Liu, J. B. Yi, Y. Yang, H. M. Fan, and J. Ding, Stable vortex magnetite nanorings colloid: Micromagnetic simulation and experimental demonstration, J. Appl. Phys. **111**, 044303 (2012).

[31] Z. K. Wang, H. S. Lim, H. Y. Liu, S. C. Ng, M. H. Kuok, L. L. Tay, D. J. Lockwood, M. G. Cottam, K. L. Hobbs, P. R. Larson, J. C. Keay, G. D. Lian, and M. B. Johnson, Spin Waves in Nickel Nanorings of Large Aspect Ratio, Phys. Rev. Lett. **94**, 137208 (2005).

[32] W. Zhang and S. Haas, Phase diagram of magnetization reversal processes in nanorings, Phys. Rev. B: Condens. Matter Mater. Phys. **81**, 064433 (2010).

[33] F. J. Castaño, C. A. Ross, C. Frandsen, A. Eilez, D. Gil, H. I. Smith, M. Redjdal, and F. B. Humphrey, Metastable states in magnetic nanorings, Phys. Rev. B: Condens. Matter Mater. Phys. **67**, 184425 (May 2003).

[34] K. Y. Guslienko and K. L. Metlov, Evolution and stability of a magnetic vortex in a small cylindrical ferromagnetic particle under applied field, Phys. Rev. B: Condens. Matter Mater. Phys. **63**, 4 (2001).

[35] P. O. Jubert and R. Allenspach, Analytical approach to the single-domain-to-vortex transition in small magnetic disks, Phys. Rev. B: Condens. Matter Mater. Phys. **70**, 144402 (2004).

[36] K. Y. Guslienko, W. Scholz, R. W. Chantrell, and V. Novosad, Vortex-state oscillations in soft magnetic cylindrical dots, Phys. Rev. B: Condens. Matter Mater. Phys. **71**, 144407 (2005).

[37] K. Y. Guslienko, V. Novosad, Y. Otani, H. Shima, and K. Fukamichi, Magnetization reversal due to vortex nucleation, displacement, and annihilation in submicron ferromagnetic dot arrays, Phys. Rev. B: Condens. Matter Mater. Phys. **65**, 244141 (2001).

[38] D. Goll, A. E. Berkowitz, and H. N. Bertram, Critical sizes for ferromagnetic spherical hollow nanoparticles, Phys. Rev. B: Condens. Matter Mater. Phys. **70**, 1 (2004).

[39] K. Y. Guslienko, V. Novosad, Y. Otani, H. Shima, and K. Fukamichi, Field evolution of magnetic vortex state in ferromagnetic disks, Appl. Phys. Lett. **78**, 3848 (2001).

[40] See the Supplemental Material at http://link.aps.org/supplemental/10.1103/PhysRevApplied.16.024002 for additional roughness-exchange-energy contribution as a function of thickness, t, in NDs and NRs, and magnetostatic energy as a function of thickness, t, in NDs.

[41] O. Zaharko, P. M. Oppeneer, H. Grimmer, M. Horisberger, H. C. Mertins, D. Abramsohn, F. Schäfers, A. Bill, and H. B. Braun, Exchange coupling in Fe/NiO/Co film studied by soft x-ray resonant magnetic reflectivity, Phys. Rev. B: Condens. Matter Mater. Phys. **66**, 1 (2002).

[42] A. Kharmouche, S. M. Chérif, A. Bourzami, A. Layadi, and G. Schmerber, Structural and magnetic properties of evaporated Co/Si(100) and Co/glass thin films, J. Phys. D: Appl. Phys. **37**, 2583 (2004).

[43] Paritosh and D. J. Srolovitz, Shadowing effects on the microstructure of obliquely deposited films, J. Appl. Phys. **91**, 1963 (2002).

[44] M. Vopsaroiu, M. Georgieva, P. J. Grundy, G. V. Fernandez, S. Manzoor, M. J. Thwaites, and K. O'Grady, Preparation of high moment CoFe films with controlled grain size and coercivity, J. Appl. Phys. **97**, 10N303 (2005).

[45] K. N. Tu, A. M. Gusak, and I. Sobchenko, Linear rate of grain growth in thin films during deposition, Phys. Rev. B: Condens. Matter Mater. Phys. **67**, 245408 (2003).

[46] T. G. S. M. Rijks, S. Lenczowski, and R. Coehoorn, In-plane and out-of-plane anisotropic magnetoresistance in thin films, Phys. Rev. B: Condens. Matter Mater. Phys. **56**, 362 (1997).

[47] M. T. Bryan, D. Atkinson, and R. P. Cowburn, Experimental study of the influence of edge roughness on magnetization switching in permalloy nanostructures, Appl. Phys. Lett. **85**, 35102 (2004).

[48] M. Kläui, C. A. F. Vaz, J. A. C. Bland, E. H. C. P. Sinnecker, A. P. Guimarães, W. Werndorfer, G. Faini, E. Cambril, L. J.

Heyderman, and C. David, Switching processes and switching reproducibility in ferromagnetic ring structures, Appl. Phys. Lett. **84**, 951 (2004).

[49] W. Casey Uhlig and J. Shi, Systematic study of the magnetization reversal in patterned Co and NiFe nanolines, Appl. Phys. Lett. **84**, 759 (2004).

[50] J. Rothman, M. Kläui, L. Lopez-Diaz, C. A. F. Vaz, A. Bleloch, J. A. C. Bland, Z. Cui, and R. Speaks, Observation of a Bi-Domain State and Nucleation Free Switching in Mesoscopic Ring Magnets, Phys. Rev. Lett. **86**, 1098 (2001).

[51] F. Garcia, H. Westfahl, J. Schoenmaker, E. J. Carvalho, A. D. Santos, M. Pojar, A. C. Seabra, R. Belkhou, A. Bendounan, E. R. P. Novais, and A. P. Guimarães, Tailoring magnetic vortices in nanostructures, Appl. Phys. Lett. **97**, 022501 (2010).

[52] J. G. Caputo, Y. Gaididei, V. P. Kravchuk, F. G. Mertens, and D. D. Sheka, Effective anisotropy of thin nanomagnets: Beyond the surface-anisotropy approach, Phys. Rev. B: Condens. Matter Mater. Phys. **76**, 174428 (2007).

[53] O. V. Pylypovskyi, D. D. Sheka, V. P. Kravchuk, and Y. Gaididei, Effects of surface anisotropy on magnetic vortex core, J. Magn. Magn. Mater. **361**, 201 (2014).

[54] W. Scholz, K. Y. Guslienko, V. Novosad, D. Suess, T. Schrefl, R. W. Chantrell, and J. Fidler, Transition from single-domain to vortex state in soft magnetic cylindrical nanodots, J. Magn. Magn. Mater. **266**, 155 (2003).

[55] E. Feldtkeller and H. Thomas, Struktur und energie von Blochlinien in dünnen ferromagnetischen schichten, Phys. Kondens. Mater. **4**, 8 (1965).

[56] S. Leulmi, H. Joisten, T. Dietsch, C. Iss, M. Morcrette, S. Auffret, P. Sabon, and B. Dieny, Comparison of dispersion and actuation properties of vortex and synthetic antiferromagnetic particles for biotechnological applications, Appl. Phys. Lett. **103**, 132412 (2013).

[57] C.-J. Jia, L.-D. Sun, F. Luo, X.-D. Han, L. J. Heyderman, Z.-G. Yan, C.-H. Yan, K. Zheng, Z. Zhang, M. Takano, N. Hayashi, M. Eltschka, M. Kläui, U. Rüdiger, T. Kasama, L. Cervera-Gontard, R. E. Dunin-Borkowski, G. Tzvetkov, and J. Raabe, Large-scale synthesis of single-crystalline iron oxide magnetic nanorings, J. Am. Chem. Soc. **130**, 16968 (2008).

[58] A. Stutzin and E. K. Hoffmann, Swelling-activated ion channels: Functional regulation in cell-swelling, proliferation and apoptosis, Acta Physiol. **187**, 27 (2006).

[59] F. Lang, M. Föller, K. S. Lang, P. A. Lang, M. Ritter, E. Gulbins, A. Vereninov, and S. M. Huber, Ion channels in cell proliferation and apoptotic cell death, J. Membr. Biol. **205**, 147 (2005).

[60] B. Martinac, Mechanosensitive ion channels: Molecules of mechanotransduction, J. Cell Sci. **117**, 2449 (2004).

[61] W. Hu, R. J. Wilson, A. Koh, A. Fu, A. Z. Faranesh, C. M. Earhart, S. J. Osterfeld, S.-J. Han, L. Xu, S. Guccione, R. Sinclair, and S. X. Wang, High-Moment antiferromagnetic nanoparticles with tunable magnetic properties, Adv. Mater. **20**, 1479 (2008).